Data Modelling for Analysis of Adaptive Changes in Fly Photoreceptors

U. Friederich, D. Coca, S.A. Billings and M. Juusola

Department of Automatic Control and Systems Engineering
The University of Sheffield
Mappin Street
S1 3JD UK

Research Report No. 995

Data Modelling for Analysis of Adaptive Changes in Fly Photoreceptors

Uwe Friederich[1,2], Daniel Coca[1], Stephen Billings[1], and Mikko Juusola[2]

[1] University of Sheffield, Department of Automatic Control and Systems Engineering, Mappin Street, Sheffield S1 3JD
[2] Department of Biomedical Science, Western Bank, Sheffield S10 2TN, UK
{u.friederich,m.juusola,s.billings,d.coca}@shef.ac.uk
http://www.shef.ac.uk/acse

Abstract. Adaptation is a hallmark of sensory processing. We studied neural adaptation in intracellular voltage responses of the R1-R6 photoreceptors, of the fruit fly *Drosophila*, subjected to light patterns of naturalistic distribution at varying intensity levels. We use experimental data in a stepwise empirical modeling procedure to estimate a non-linear dynamical model (NARMAX) with variable gain. This model can describe accurately the observed adaptation process at each new level of changing light inputs. Generalized frequency response functions were used to visualize and quantify adaptation in the frequency domain.

Key words: Non-linear system identification; NARMAX; Generalized frequency response functions; Neural adaptation; Gain adaptation; *Drosophila*; Naturalistic stimulation

1 Introduction

Adaptation enables efficient encoding of sensory information in single neurons or neural chains. This it does by tuning the system's input-output relationship so that the neural output can best represent sensory information [1–4]. For example, although light intensity in a single natural scene can vary thousand-fold [5], photoreceptors have no difficulties in encoding these patterns. Despite their limited dynamic range[1], photoreceptors can discriminate contrast over the full extend of light levels [5]. Because our understanding of the underlying physiological processes of phototransduction is limited, so are our biophysical models. Therefore, empirical modeling methods have a great value in comprehending the system's overall neural functions and in producing hypothetical models that can be tested experimentally.
Starting with the pioneering work of Marmarelis and McCann in the early 1970s [6, 7], various authors have applied non-linear system analysis to study nonlinear dynamics in early visual neurons. The most common approach has been

[1] Dynamic range: Here defined as the ratio of the maximum response and the noise level

the identification of Volterra kernels based on the Cross-Correlation method [8, 9] or the sum-of-sinosoids method [10, 11]. Both methods have been strongly restricted in the selection of the stimuli, to be either a mixture of sinosoids or Gaussian White Noise (GWN). The latter has been shown to linearise fly photoreceptor outputs and does not excite its nonlinear dynamics as natural scenes do [12, 5]. Motivated by this observation, van Hateren developed a model that is able to simulate fly photoreceptor responses to natural light statistics [13]. However, in this study, the light stimuli was limited to a 2-3 log unit range and the model itself had a fixed structure. To study adaptive gain regulation, a more flexible model structure is desirable. Whilst new kernel based methods [14, 15] are not restricted in the input distribution anymore, large training data sets are still required for the estimation of higher order kernels. Moreover, the analysis of estimated models is restricted to the analysis of kernel shapes, from which a physical meaning can only be indirectly inferred.

To avoid difficulties encountered in previous studies, we employ a well established nonlinear system identification methodology developed for NARMAX (Nonlinear Auto Regressive Moving Average with eXogenous inputs) models, that has not been applied to study neural systems before. The NARMAX approach allows the identification of parametric models from small data sets, independent of the input data statistics. This makes it a very attractive method to study fast neural adaptation. Once a model has been identified, it can be analytically transformed into generalized frequency response functions (GFRF). The combined approach allows the study of the system dynamics in both, the time and the frequency domain. Analysis on GFRF provide a tool for studying how adaptation changes the frequency dependent interactions between the input and output.

Based on the NARMAX methodology, we estimated models that can accurately predict photoreceptors' voltage responses to temporal light patterns of naturalistic distribution [5]. Individual models were estimated for light levels ranging in logarithmic steps 10,000 fold. Analysis on GFRF allowed us to find a combined model structure and a single parameter set to approximate adaptive changes by a pure change in the input gain.

The data for this study has been acquired from the "small" fly, *Drosophila*, rather than from previously used "big" flies to make use of its extensive genetic and molecular toolbox [16]. Targeted manipulation at each neural layer of the flies visual system will allow us in a later stage of this study to obtain more insight which neural interactions (*e.g.* lateral synaptic connections, feedback from higher order cells, etc.) influence adaptation and how.

2 Methodology

2.1 Measurements and Stimuli

Wild-type Canton-S strains of *Drosophila* were used in the experiments. The flies were prepared *in vivo* as in [17]. Intracellular voltage responses of blue-green-sensitive R1-R6 photoreceptor cells were recorded using sharp quartz

microelectrodes. Photoreceptors were excited by a point of light at the center of their receptive field, as delivered through liquid light guides, connected to high performance LEDs (Fig.3(a)). The measured linear light output of the LEDs was taken as the input to the photoreceptors. Light patterns were selected from the van Hateren's natural-stimulus-collection, (`http://hlab.phys.rug.nl/archive.html`) [5]. The stimuli was played back at 2 kHz and measured by a photo diode circuit. Voltage responses (output) and light stimuli (input) were low-pass filtered with a cutoff at 1 kHz before sampling with 2 kHz, and stored for off-line analysis. Light input was attenuated by neutral density filters. This attenuation was performed very rapidly (< 0.1 ms) during the experiments (Fig. 1).
To test the range of adapting inputs, the same temporal light pattern was shown to the fly with 0, 1, 2, 3 and 4 log intensity units attenuation, allowing 5 different adaptive levels, named as BG0-BG4; BG0 = very bright, BG4 = very dim. Stimulation at each light level lasted for 20 s (Fig. 1). Within this time, a 2 s pattern was repeated for us to quantify data variation.

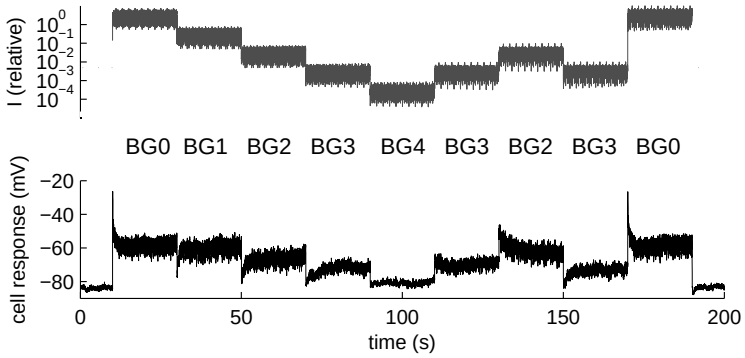

Fig. 1. (top) Relative light intensity values (top) and corresponding photoreceptor responses (bottom). Sections of individual light levels are marked as BG0 (very bright) to BG4 (very dim)

2.2 Data Pre-Processing

For system identification, it is essential that the bandwidth of the excitatatory signal does not extensively exceed that of the system under study [18]. It has been shown before that for white noise stimulation, *Drosophila* photoreceptors can follow inputs with $\lesssim$ 100 Hz [17]. However, naturalistic stimuli evokes larger responses and might extend the bandwidth [19]. For this reason the input and output data sequences were pre-filtered by a Butterworth low-pass filter with a 200 Hz cut-off. Subsequently, the data has been down-sampled to 400 Hz [18].

2.3 Signal to Noise Ratio

Neural recordings are generally noisy because biochemical reactions are probabilistic rather than deterministic processes. Additionally, recordings from *Drosophila* photoreceptors are particularly sensitive to measurement noise, because the tiny cell dimensions make stable recordings difficult. Moreover, at low light intensity stimulation, photon shot noise has a significant influence on the stimuli and therefore indirectly effects the photoreceptor outputs [3].
The quality of modelling directly depends on the noise level in the data. Therefore we quantify the Signal to Noise Ratio (*SNR*) of the output for each input light level. Because the number of repetitions is limited, we apply an bias corrected *SNR* estimation procedure [20, 13]. We estimate the signal $y_{raw} = \overline{y}$ by the ensamble average as $\overline{y} = \frac{1}{J}\sum_{i=1}^{J} y_i(t)$ from measured responses $y_i,\ i = 1...J$ to J repeated stimuli. Adopting the notation in [13], we obtain the raw signal and noise power in the voltage output by

$$P_{S_{raw}} = \frac{1}{T}\int_0^T \overline{y}^2(t)dt \quad \text{and} \quad P_{N_{raw}} = \frac{1}{J}\sum_{i=1}^{J}\frac{1}{T}\int_0^T (y_i(t) - \overline{y})^2(t)dt \ , \tag{1}$$

and the bias corrected signal and noise power estimate by

$$\hat{P}_S = P_{S_{raw}} - \frac{1}{J}\hat{P}_N \quad \text{and} \quad \hat{P}_N = \frac{N}{N-1}P_{N_{raw}} \ . \tag{2}$$

Thus, the here applied SNR estimate is given by the ratio of the bias corrected signal power over the power of noise

$$SNR = \frac{\hat{P}_S}{\hat{P}_N} \ . \tag{3}$$

2.4 NARMAX Modeling Methodology

NARMAX is a methodology to estimate and validate nonlinear difference equation models purely from observations of a system's response to its environmental stimuli. Since the introduction of the NARMAX model by Billings and Leontaritis [21, 22], it has been successfully applied in the identification and analysis of a wide range of engineering, biomedical and financial systems. The NARMAX model, is given as

$$\begin{aligned} y(t) = f(&y(t-1), ..., y(t-n_y), u(t-1), ... \\ &..., u(t-n_u), e(t-1), ..., e(t-n_e)) + e(t) \ , \end{aligned} \tag{4}$$

where $y(t)$, $u(t)$ and $e(t)$ are the sampled system output, input and error sequences, respectively. $f(\cdot)$ is the nonlinear mapping vector; n_y, n_u and n_e are the maximum lags in the output, input and noise. The noise variable $e(t)$ is a zero mean independent sequence, which accommodates the effects of measurement noise, modeling errors and unmeasured disturbances. $e(t)$ is often referred to

as the prediction error, which is defined as $e(t) = y(t) - \hat{y}(t)$, where $\hat{y}(t)$ is the one step ahead prediction of $f(\cdot)$. In this study, $f(\cdot)$ has a l-order polynomial structure with a single input and output (SISO), such that equation (4) becomes

$$\begin{aligned} y(t) = \theta_0 + \sum_{i_1=1}^{n} \theta_{i_1} x_{i_1}(t) + \sum_{i_1=1}^{n} \sum_{i_2=i_1}^{n} \theta_{i_1,i_2} x_{i_1}(t) x_{i_2}(t) + ... \\ ... + \sum_{i_1=1}^{n} \dots \sum_{i_l=i_{l-1}}^{n} \theta_{i_1,\dots,i_l} x_{i_1}(t) ... x_{i_l}(t) + e(t) \ , \end{aligned} \tag{5}$$

where $x(t)$ denotes the lagged variables in y, u and e. n is the sum of variables $n = n_y + n_u + n_e$, and θ_i are scalar parameters to be estimated. Hammerstein, Wiener, Bilinear and Volterra models that have been previously applied to model neural systems are all subclasses of the polynomial NARMAX model and can be derived from (5) [23].
The prediction error terms $e(.)$ are included in the NARMAX model to accommodate noise. Although in this paper we apply no further analysis on the noise model, it is estimated to ensure the process model is unbiased.
In the here applied method , we apply parameter estimation, structure detection and model validation in an interlinked procedure [24].

- **Term Selection & Parmeter Estimation by the OLS Algorithm**. The model structure (5) is linear in its parameters θ_i, this allows the construction of a linear regression model in matrix form,

$$y(t) = \sum_{i=1}^{M} p_i(t)\theta_i + e(t), \quad t = 1...N \qquad \text{or} \qquad \mathbf{y} = \mathbf{P\Theta} + \epsilon \ , \tag{6}$$

  where N denotes the length of the training data set, the $p_i(t)$ are monomials (terms) of $x_1(t)$ to $x_n(t)$ up to degree l. The modelling error sequence ϵ is iteratively obtained. $\mathbf{\Theta} = [\theta_{\mathbf{0}}, ..., \theta_{\mathbf{i_1},...,i_l}]^{\mathbf{T}}$ is the M-dimensional parameter vector to be estimated.
  Under the condition that $\mathbf{P}$ has full rank, the Orthogonal Least Squares (OLS) algorithm [25] applies an orthogonal decomposition of the regression matrix, such that $\mathbf{P} = \mathbf{WA}$, with $\mathbf{W}$ being an orthogonal matrix, satisfying $\mathbf{D} = \mathbf{W^T W}$, where $\mathbf{D}$ is $diag(d_1, ..., d_M)$. Equation (6) is therefore equivalent to $\mathbf{y} = \mathbf{Wg} + \epsilon$, with $\mathbf{g} = \mathbf{A\Theta}$. Instead of estimating $\mathbf{\Theta}$ directly, $\hat{\mathbf{g}}$ is estimated as the linear least squares solution that minimizes $\|\mathbf{y} - \mathbf{Wg}\|$, where $\|.\|$ is the euclidean norm. $\mathbf{W}$ being orthogonal allows to calculate each element g_i (for the i^{th} term) in $\hat{\mathbf{g}}$ independently. The error reduction ratio $ERR_i = \frac{g_i^2 d_i}{\mathbf{y}^T, \mathbf{y}}$ is used to evaluate for each g_i, how much the corresponding term contributes to the output. In a forward regression manner, terms are chosen first that contribute more to the output until the selection is stopped, when all significant terms are selected. In general only a small number of terms $m << M$ is enough for approximating the systems dynamics [25]. Eventually, the parameter estimates are calculated from $\hat{\mathbf{\Theta}} = \mathbf{A^{-1}}\hat{\mathbf{g}}$.

- **Model Validation** Cross validation was used to evaluate the model performance on unseen data. This ensures that the model describes the underlying dynamical process and not just the training data. Models are selected and validated, based on the performance in the following complementary tests.
  · *Normalized Mean Square Error (NMSE)*

$$NMSE = \frac{\sum_{t=1}^{N_d} \left(\hat{y}(t) - y(t)\right)^2}{\sum_{t=1}^{N_d} \left(y(t) - E[y]\right)^2} \ , \tag{7}$$

  where $E[y] = \frac{1}{N_d} \sum_{t=1}^{N_d} y(t)$ is the mean of the measured output, N_d is the validation data length and $\hat{y}(t)$ are the model predictions. Depending, if the predictions are purely model predicted outputs, $\hat{y}(t) = \hat{y}(t)_{MPO}$ or one step ahead predictions $\hat{y}(t) = \hat{y}(t)_{OSA}$, the $NMSE_{MPO}$ or the $NMSE_{OSA}$ are evaluated.
  · *Final Prediction Error (FPE)* [26]

$$FPE = \frac{N_d + m\gamma}{N_d - m\gamma} \sigma_e^2 \ , \tag{8}$$

  where σ_e^2 is the variance of the error sequence $e(t) = y(t) - \hat{y}(t), \quad t = 1...N_d$ and m is the number of selected terms. The measure is used to reduce the spread of the error penalized by the model size.
  · *Higher order correlation tests*

$$\begin{aligned} \Phi_{(\epsilon^2)'(y\epsilon)'}(\tau) &= \kappa\delta(\tau) \ \forall\tau \\ \Phi_{(u^2)'(y\epsilon)'}(\tau) &= 0 \qquad \forall\tau \ , \end{aligned} \tag{9}$$

  where κ is a constant $0 < \kappa < 1$ and Φ_{vw} is the normalized correlation function of signal v and w. The dash, (.)', denotes that the mean level of the signal in the brackets is removed. The shift between v and w has been selected to be $\tau = -100...100$. The visual tests show, if (within a 95% confidence interval) the residuals contain dynamics different from Gaussian White noise that are not yet captured by the NARMAX model [27].

Estimation and validation algorithms have been implemented in MATLAB®, allowing a consistent modelling approach for all models that are part of this study. Although, all models have been validated by each of the described measures, for clarity, in the results section only the NMSE is shown.

2.5 Generalized Frequency Response Functions

The NARX model, a subset of the NARMAX, containing functionals of lagged inputs and outputs alone, can (under some assumptions) be expanded into a Volterra functional polynomial of the input $u(t)$ only [28]. The discrete Volterra Series is defined as, [29],

$$y(t) = \sum_{n=1}^{\infty} y_n(t) \ , \tag{10}$$

where $y_n(t)$ denotes the n-th order output of the system and is given by,

$$y_n(t) = \sum_{0}^{t} ... \sum_{0}^{t} h_n(k_1, ..., k_n) \prod_{i=1}^{n} u(t - k_i) \ , \tag{11}$$

where $h_n(k_1, ..., k_n)$ is called the 'n-th order kernel' or the 'n-th order impulse response' of the system. The multidimensional Fourier transform of the n-th order impulse response $h_n(k_1, ..., k_n)$ yields the n-th order transfer function or the'n-th order Generalized Frequency Response Function (GFRF)

$$H_n(j\omega_1, j\omega_2, ..., j\omega_n) = \sum_{\omega_1=-\infty}^{\infty} ... \sum_{\omega_n=-\infty}^{\infty} h_n(k_1, ..., k_n) e^{-j(\omega_1 k_1 + ... + \omega_n k_n)} \ . \tag{12}$$

The first order GFRF, $H_1(j\omega)$ explains linear effects, while the nonlinear GFRF's, $H_n(j\omega_1, ..., j\omega_n)$ $n > 1$, give a measure of the nonlinear coupling of the input spectral components and reveal energy transfer mechanisms to new spectral components in the output [30].
For this study, GFRF have been analytically computed directly from identified discrete time NARX models, applying the recursive algorithm developed by Peyton Jones and Billings [31]. In contrast to the direct estimation of GFRF from input output data, this method requires significantly less data samples.

3 Results

We measure voltage responses in *Drosophila* photoreceptors to naturalistically distributed light contrast time series (Fig. 3(a)). The same light pattern was repeated at different light levels (BG0-BG4). BG0 is the brightest level; BG1 gives the same pattern but 10-times less intense; BG2 is 100-times weaker than BG0, etc (Fig. 1). From the corresponding light input and photoreceptor voltage output, NARMAX models were estimated and mapped into the frequency domain as GFRFs. Data analysis and model identification are implemented as a four step procedure.

Step 1: *SNR* estimation of voltage outputs at each BG level.
Step 2: Identification of local NARMAX models, at each BG level separately (M_{BG0} to M_{BG3}).
Step 3: Identification of a global model structure that can explain the complete data set by adjusting its parameters ($M_G(\Theta_{BG1})$ to $M_G(\Theta_{BG3})$).
Step 4: Identification of a global model that can explain the complete data set by adjusting only its input gain, α ($M_G(\Theta_G, \alpha_1)$ to $M_G(\Theta_G, \alpha_3)$).

Models are estimated from training data sets, containing 800 input/output samples. All shown NMSE values are based on 6400 output predictions, simulated by models that performed best in all validation tests. These values are used as a performance index to compare models.

3.1 Data Variability Analysis

For each BG level, the *SNR* (3) has been calculated from voltage responses to $J = 8$ input repetititons. The results, summarized in Table 1 show a significant decay of signal Power $\hat{P_S}$ in comparison to noise Power $\hat{P_N}$, as the light intensity decreases. Consequently, the *SNR* values drop in the same manner. At lower

	BG0	BG1	BG2	BG3	BG4
$\hat{P_S}$	9.13	10.02	7.66	2.71	0.247
$\hat{P_N}$	0.37	0.53	0.69	0.80	0.68
SNR	24.91	18.87	11.03	3.40	0.36

Table 1. Signal power, noise power Signal to Noise Ratio (3) at distinct BG levels

light intensities, less photons are available to activate the phototransduction cascade, which leads to smaller voltage responses [32]. At the same time stochastic photon capture in the photoreceptors induces additional randomness and decreases the *SNR* at lower light levels. This trend resembles the results shown previously in [33]. Because noise in the input or in the output cannot be simulated, model predictions deviate from output measurements, even if a model captures perfectly the underlying system. This has a direct implication on any prediction error based validation test. Therefore, data with low *SNR* values inevitably lead to higher NMSE values. For this reason models estimated from input/output data at dimmer light levels inevitably show poorer performance than models at bright light intensities.

3.2 Individual Model Estimation at each BG Level

In this part of the study, the structure and parameters of NARMAX models were individually estimated from stimuli-response data BG0 to BG3 (*cf.* Fig. 1). For BG4, no reliable model could be found. The low $SNR = 0.558$ suggests that for this dim inputs the photoreceptors cannot discriminate light patterns anymore from noise and produce mostly random quantum fluctuations [17].
Table 2 contains models M_{BG0} (bright input) to M_{BG3} (dim input) and their performance index (*NMSE*). NMSE values show that models estimated from responses to brighter inputs (M_{BG0} to M_{BG2}) predict remarkably well throughout the same light level, even for data sets that were not used for estimation. Significantly poorer performs the model M_{BG3}, this can be explained by the low *SNR* at the dim light level.
Throughout all the tested light levels, second order polynomial models are sufficient to model the observed dynamics of the underlying nonlinear system. Higher order polynomial models were also investigated, but these did not improve the model performance. Despite the input changes by 3 log units, the structures of models M_{BG0} to M_{BG3} (Table 2) are very similar. Terms in models of different BG levels vary mostly in $+/-$ one lag. The strong similarity in the set of detected terms for models of different light levels suggests that a global model structure can explain the data for all tested input levels.

terms \ models	M_{BG0}	M_{BG1}	M_{BG2}	M_{BG3}	$M_G(\Theta)$
offset	-58.42	-59.75	-66.39	-72.2423	
c	-2.026	-2.309	-1.792	-0.616	$\hat{\theta}_0$
y(t-1)	0.964	1.009	1.089	0.949	$\hat{\theta}_1$
y(t-2)	–	-0.154	-0.209	–	
y(t-3)	0.173	–	–	–	$\hat{\theta}_2$
y(t-4)	-0.348	–	–	–	$\hat{\theta}_3$
y(t-5)	0.093	–	–	0.135	$\hat{\theta}_4$
u(t-4)	0.165	1.551	17.15	–	$\hat{\theta}_5$
u(t-5)	0.279	3.857	27.06	–	$\hat{\theta}_6$
u(t-6)	0.257	3.523	21.90	132.83	$\hat{\theta}_7$
u(t-7)	0.126	–	–	–	$\hat{\theta}_8$
y(t-1)u(t-5)	–	–	-1.319	37.58	
y(t-2)u(t-4)	-0.030	0.311	–	-12.778	$\hat{\theta}_9$
y(t-2)u(t-5)	–	–	–	-38.5616	
y(t-5)u(t-4)	0.051	0.671	–	–	$\hat{\theta}_{10}$
y(t-5)u(t-5)	–	–	0.487	–	
y(t-6)u(t-4)	-0.039	-0.635	-0.881	–	$\hat{\theta}_{11}$
u(t-3)u(t-7)	0.012	–	–	–	$\hat{\theta}_{12}$
u(t-4)u(t-5)	-0.015	-0.399	-87.15	–	$\hat{\theta}_{13}$
u(t-5)u(t-6)	–	-4.420	-89.13	-8602	
u(t-6)u(t-7)	-0.028	–	–	2466	$\hat{\theta}_{14}$
$NMSE_{MPO}$	0.094	0.083	0.096	0.254	
$NMSE_{OSA}$	0.016	0.018	0.027	0.067	

Table 2. Independently estimated NARMAX models for different light levels. Model parameters are presented in columns. The first column contains corresponding terms for each parameter. "-" denotes that a term was not selected. The last column contains the global model structure $M_G(\Theta)$.

3.3 Parameter Estimated Models with Constant Structure

Various combinations of terms in Table 2 were tested to construct a global model structure that performs well at all BG levels. The best structure was found to be the previously detected M_{BG0} term set. Adopting the structure from M_{BG0}, the global structure is called $M_G(\Theta_{BGi})$ with $\Theta_{BGi} = [\hat{\theta}_0^{BGi}, ..., \hat{\theta}_{14}^{BGi}], i = 0, ..., 3$, being the model parameters estimated individually at light levels BG0-3. Table 3 summarizes the results for individually estimated parameter sets, from input/output data at light levels BG0-3.

At all tested light levels, the model performance does not decrease for keeping a global model structure, compared to values of models with individually

Uni Model	$M_G(\hat{\Theta}_{BG0})$	$M_G(\hat{\Theta}_{BG1})$	$M_G(\hat{\Theta}_{BG2})$	$M_G(\hat{\Theta}_{BG3})$
$NMSE_{MPO}$	0.094	0.067	0.096	0.23
$NMSE_{OSA}$	0.016	0.017	0.025	0.064

Table 3. Performance of models with global structure and BG-dependent parameter estimates

estimated structures. For dimmed inputs, parameter estimated models with a constant structure even perform slightly better. This suggest that a single nonlinear model with varying parameters indeed can be used to describe the input-output data set.
To investigate adaptative changes in the frequency domain, the first and second order GFRF's $H_{1,BGi}(j\omega)$ and $H_{2,BGi}(j\omega_1, j\omega_2)$, $i = 0..3$ were computed for the identified NARMAX models $M_G(\Theta_{BG0})$ to $M_G(\Theta_{BG3})$, respectively. Fig. 2 summarizes the results in plots of the first-order functions (Fig. 2(a)) and selected slices through second-order functions (Fig. 2(c), 2(d)). The location of slices is shown in Fig. 2(b). Analysis on the first and second order GFRF magnitude plots

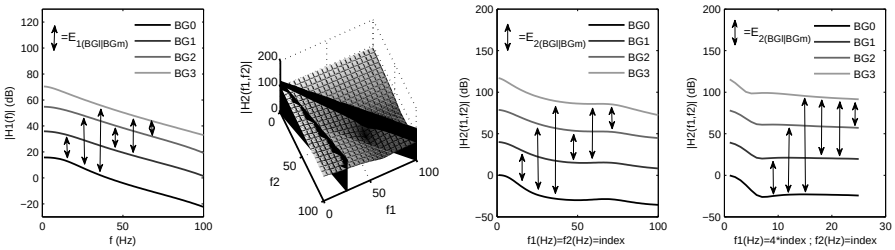

(a) 1^{st} order GFRF (b) slice locations 2^{nd} order GFRF (c) 2^{nd}order GFRF slice 1 (d) 2^{nd} order GFRF slice 2

Fig. 2. 1st order GFRF plots of and slices through 2nd order GFRF for models $M_G(\Theta_{BG1})$ to $M_G(\Theta_{BG3})$. Changes between frequency responses of different light levels are indicated by arrows

in Fig. 2 reveal that the $3dB$ bandwidth of the system remains constant, at about 20 Hz, regardless of the light level. An energy transference phenomenon like described in [30] is not eminent. For decreasing intensity levels, the magnitude curves are shifted upwards whilst their shape remains almost the same. This suggests that the photoreceptor adaptation to lower light intensities is manifested just through an increase of the input gain. If this hypothesis is correct then we would expect that the second order magnitude plots will be shifted upwards by an amount equal to the squared linear shift.
Indeed, assuming the Volterra Series in (10) is expanded up to the second order kernel, then its Fourier transform yields, [34],

$$Y_1(j\omega_1, j\omega_2) = H_1(j\omega_1)U(j\omega_1) + H_2(j\omega_1, j\omega_2)U(j\omega_1)U(j\omega_2) \ , \tag{13}$$

where $H_1(.)$ and $H_2(.)$ are the first and second order GFRF in (12) and $Y(.)$ and $U(.)$ are the Fourier Transforms of the output and input, respectively. Assuming, the input signal is modified by a constant gain α, then (13) yields,

$$Y_2(j\omega_1, j\omega_2) = H_1(j\omega_1)\underline{\alpha U(j\omega_1))} + H_2(j\omega_1, j\omega_2)\underline{\alpha U(j\omega_1)\alpha U(j\omega_2))} \tag{14}$$

$$\Leftrightarrow Y_2(j\omega_1, j\omega_2) = \underline{\alpha H_1(j\omega_1)}U(j\omega_1)) + \underline{\alpha^2 H_2(j\omega_1, j\omega_2)}U(j\omega_1)U(j\omega_2)) \ , \tag{15}$$

where $Y_1(.) \neq Y_2(.)$. The underlines in equations (14) and (15) highlight that in a second order Volterra Model, a change in the input signal by a constant gain α is equivalent to a constant gain α in $H_1(.)$ and a quadratic gain α^2 in $H_2(.)$. To test, if this is the case for changes in GFRF's of models $M_G(\Theta_{BG0})$ to $M_G(\Theta_{BG3})$, we calculated α as the arithmetic mean $E_{BGl|BGm}$ of shifts between first order GFRF curves $H_{1,BGl}(.)$ and $H_{1,BGm}(.)$ $l, m = 0..3$ as

$$E_{1(BGl|BGm)} = \frac{1}{\omega_{max}} \sum_{\omega=1}^{\omega_{max}} H_{1,BGl}(j\omega) - H_{1,BGm}(j\omega) \ . \tag{16}$$

These, we compared to corresponding mean shifts between second order GFRF surfaces calculated as

$$E_{2(BGl|BGm)} = \frac{1}{\omega_{max}^2} \sum_{\omega_1=1}^{\omega_{max}} \sum_{\omega_2=1}^{\omega_{max}} (H_{1,BGl}(j\omega_1, j\omega_2) - H_{2,BGm}(j\omega_1, j\omega_2) \ , \tag{17}$$

where $H_{2,BGi}(.)$ denotes the second order GFRF of model $M_G(\Theta_{BGi})$, $i = 0...3$. According to previous argumentation, for a pure change in input gain, $E_{2(BGl|BGm)} \approx \alpha^2$ needs to be satisfied for all combinations of $l, m = 0...3$. To test this, we transformed the second order shift into α^p with $p = \frac{log(E_{1(BGl|BGm))}}{log(E_{2(BGl|BGm))}}$. As a measure, how much curves deviate from being a pure shift, we additionally calculated the variance between differences of GFRFs as

$$\sigma^2_{1(BGl|BGm)} = \frac{1}{\omega_{max}} \sum_{i=1}^{\omega_{max}} (H_{1,BGl}(j\omega) - H_{1,BGm}(j\omega) - E_{BGl|BGm})^2 \qquad \text{and} \tag{18}$$

$$\sigma^2_{2(BGl|BGm)} = \frac{1}{\omega_{max}^2} \sum_{\omega_1=1}^{\omega_{max}} \sum_{\omega_2=1}^{\omega_{max}} (H_{1,BGl}(j\omega_1, j\omega_2) - H_{2,BGm}(j\omega_1, j\omega_2) - E_{2(BGl|BGm)})^2.$$

Results of the evaluation of shifts between first and second order GFRF functions for $\omega_{max} = \frac{100Hz}{2\pi}$ are summarized in Table 4. The analysis of the 2nd order

(l, m)	$(0,1)$	$(0,2)$	$(0,3)$	$(1,2)$	$(1,3)$	$, (2,3)$
$\alpha = E_{1(BGl\|BGm)}$	22.66dB	41.37dB	53.95dB	18.70dB	31.29dB	12.58dB
$\alpha^p = E_{2(BGl\|BGm)}$	43.81dB	82.31dB	117.0dB	38.50dB	73.17dB	34.67dB
$\sigma^2_{1(BGl\|BGm)}$	2.05dB^2	1.84dB^2	0.60dB^2	0.10dB^2	0.95dB^2	0.93dB^2
$\sigma^2_{2(BGl\|BGm)}$	3.91dB^2	4.94dB^2	12.34dB^2	1.38dB^2	10.68dB^2	5.93dB^2
p	1.93	1.99	2.16	2.06	2.33	2.75

Table 4. Evaluation of adaptive changes between GFRFs of models $M_G(\Theta_{BGl})$ and $M_G(\Theta_{BGm})$, estimated from data at the l^{th} and m^{th} light level BGl and BGm (arrows Fig.2).

GFRF magnitudes reveal that indeed the shifts in this case have a quadratic tendency relative to the linear shifts. Only shifts to GFRFs of model $M_G(\Theta_{BG3})$ deviate. The shift between the linear GFRF of $M_G(\Theta_{BG2})$ and its 2nd order one is almost cubic ($\alpha^{2.75}$). There could be two reasons for this deviation. If, the shifts to GFRFs for light level BG3 are accurate then, at very dim light levels the nonlinear contribution the output signal enhances. Alternatively, if the high amount of noise at dim light levels leads to biased parameter estimates, causing corresponding GFRFs to be inaccurate while the system in fact would perform

pure gain adaptation. In case of the latter, the system performs a normalization of its frequency response at different input light levels, by holding on to a constant spectral characteristic. By adjusting a gain, it maintains the response amplitude within the limited range of 50 mV, while the same frequencies in the output are kept constant throughout all the tested BG levels.

3.4 Global Model with Gain Adaptation

Frequency normalization in the form of a pure gain adaptation can be modelled by a global model structure with a constant global parameter set $\mathbf{\Theta_G}$ and a variable input gain α. Indeed, instead of a shifting the GFRF $H_1(.) \rightarrow \alpha H_1(.)$ and $H_2(.) \rightarrow \alpha^2 H_2(.)$ as in (15), the input can be altered by a constant gain $U(.) \rightarrow \alpha U(.)$ as in (14). The same can be shown in the time domain, considering the inverse Fourier Transform of $\alpha U(j\omega) = \alpha u(t)$. Assuming, there exists a unique transformation between a Volterra-Model and a polynomial NARX-Model [35, 28], then it can be shown for a polynomial NARX model (5) that a change of the input variable by a constant α, such that $u(t) \rightarrow \alpha u(t)$, is equivalent to a shift by α, in its first order GFRF, by α^2, in its 2nd order GFRF, etc (*cf* proof in [28]).
Motivated by this finding and results, shown in Table 4, we constructed a global model, to explain the full input-output data set by adapting only one parameter[2], the input gain α. The global model consists of the global model structure $M_G(\Theta_G) = M_B G0$, with the best tested parameter set $\Theta_G = \Theta_{BG0}$ and an adjustable input gain α_i, such that $u(t) \rightarrow \alpha_i u(t)$, where the index "$_i$" refers to the i^{th} light level *BGi*. Therefore, $M_G(\Theta_G, \alpha_i)$ denotes the global model. Table 5 summarizes the performance of the global model for predicting the output at each light level BG0-3. The parameters α_i , $i = 0...3$ have been estimated using the MATLAB® implementation of the L-M algorithm. The global Model

Uni Model	$M_G(\Theta_G, \alpha_0)$	$M_G(\Theta_G, \alpha_1)$	$M_G(\Theta_G, \alpha_2)$	$M_G(\Theta_G, \alpha_3)$
α_i	1=0dB	11.80=21.4dB	79.14=38.0dB	290.4=49.3dB
$NMSE_{MPO}$	0.094	0.081	0.106	0.239
$NMSE_{OSA}$	0.016	0.018	0.028	0.07

Table 5. Performance of global model with BG-dependent input gain α

$M_G(\Theta_G, \alpha_i)$, $i = 0...3$ performs almost as good at each BG level, as if the full set of parameters $\hat{\mathbf{\Theta}}$ is estimated independently at each light level (*cf* Table 3). Although, the 2nd order GFRF calculated from the parameter estimated model $M_{BG3}(\Theta_{BG3})$ was not exactly quadratic, however, forcing a quadratic change by a global model, does not significantly decrease the models performance, measured by the *NMSE*. It is therefore possible that even at very dim light levels, like BG3, the system performs a frequency normalization. This result suggests that the input-output data can, within its limitations at low light levels,

[2] Note: Adjustments to small variations in the output offset have been applied. Since these small adjustments do not change the results they are not further discussed here.

be described by the suggested global model with light level dependent adjusted input gain α.

4 Discussion

In this paper, nonlinear system identification and analysis techniques were used to investigated the adaptation of *Drosophila* photoreceptors to different light intensity levels. Instant changes between light levels cause the system to respond in distinct adaptive modes, so as to discriminate light patterns, which can vary 10,000 fold. Such coding occurs reliably within the limited voltage range (50-60 mV) of photoreceptors.
For the first time, a unified nonlinear dynamical model of the photorecetor that explains adaptation at each level of dynamic light inputs as a simple gain adjustment process was derived using nonlinear system identification based on experimental measurements of photoreceptor responses to naturalistic stimuli. The use of generalized frequency response functions was instrumental in revealing the underlying mechanism of this type of adaptation. The derived model was validated extensively using data sets recorded for different light levels. The graph shown in Fig. 3(b) summarizes the performance of all the estimated models and highlights that the same model performance could be achieved for individual estimated models, models with fixed structure, and the global model with an adapted gain. The individual model performances are remarkably good when compared to the natural data variation, measured by its *SNR*. Fig. 3 shows the model predictions of parameter and gain adapted models in comparison to the actual recorded voltage responses.
We showed that *Drosophila* photoreceptors adapt to changing light inputs to

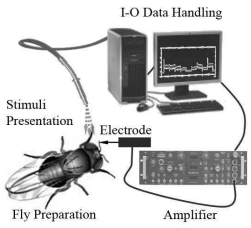

(a) Experimental Setup

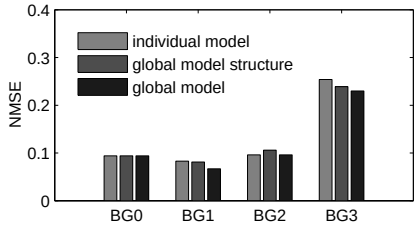

(b) NMSE comparison of different modeling approaches

preserve the spectral structure in its output to higher order neurons. These dynamics are quite different from those shown previously for Gaussian White Noise inputs [17], where the system integrated the dim and differentiated the bright inputs. Instead, when *Drosophila* photoreceptors adapt to naturalistic contrasts, it appears that they employ a pure gain control. This was tested by simulating the system with fixed NARMAX model, whilst only optimizing the

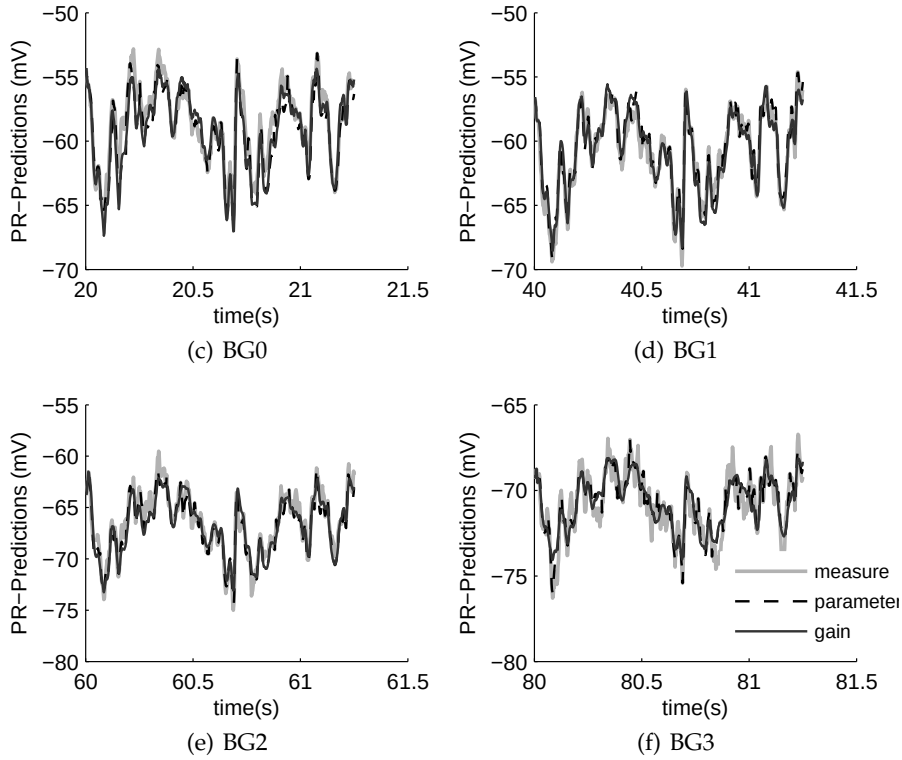

(c) BG0 (d) BG1

(e) BG2 (f) BG3

Fig. 3. Evaluation of model predicted outputs $\hat{y}_{MPO}$ at different background light intensities for gain- and parameter adjusted models

input gain. These new findings have implications on the understanding how insect eyes code visual information. To learn more about the nature of adaptation, similar experiments, involving visually impaired fly mutants will be carried out. By replacing the constant gain with a variable gain, we will be able to use the derived global model in future studies to investigate the influence of stimulation patterns with different statistics onto adaptation.

Acknowledgement We thank H.van Hateren for providing the naturalistic time series of light intensities. This work was supported by the Biological Sciences Research Council (BBF0120711 and BBD0019001 to MJ). DC and SAB gratefully acknowledge that this work was supported by the Engineering and Physical Sciences Research Council and the European Research Council. UF readily acknowledges the support by the University of Sheffield.

References

1. Barlow, H. *Possible principles underlying the transformation of sensory messages.* Sensory Communication. MIT Press, (1961).

2. Nikolaev, A., Zheng, L., Wardill, T., O'Kane, C., de Polavieja, G., and Juusola, M. *PLoS ONE* **4**(1), – (2009).
3. van Hateren, J. *Biol. Cybern.* **68**(1), 23–29 (1992).
4. Wark, B., Lundstrom, B. N., and Fairhall, A. *Current Opinion in Neurobiology* **17**(4), 423–429 August (2007).
5. Van Hateren, J. *VIS. RES.* **37**(23), 3407–3416 (1997).
6. Marmarelis, P.Z.; Naka, K.-I. *Science* **175**, 1276–1278 (1972).
7. McCann, G. *Jurnal of Neurophysiology* **37**, 869–895 (1974).
8. Eckert, H. and Bishop, L. *Biological Cybernetics* **17**(1), 1–6 (1975).
9. Marmarelis, V. and McCann, G. *Biological Cybernetics* **27**(1), 57–62 (1977).
10. Victor, J., Shapley, R., and Knight, B. *PROC. NATL. ACAD. SCI. U. S. A.* **74**(7), 3068–3072 (1977).
11. Victor, J. *Proc Natl Acad Sci U S A* **76**(2), 996–998 (1979).
12. Juusola, M., Kouvalainen, E., Jarvilehto, M., and Weckstrom, M. *Journal of General Physiology* **104**(3), 593–621 (1994).
13. Van Hateren, J. H. and Snippe, H. P. *Vision Research* **41(14)**, 1851–1865. (2001).
14. Marmarelis, V. *Nonlinear Dynamic Modeling of Physiological Systems*. Wiley Interscience, (2004).
15. Korenberg, M. and Hunter, I. *Ann Biomed Eng* **24**(2), 250–268 (1996).
16. Borst, A. *Current Biology* **19**(1), – (2009).
17. Juusola, M. and Hardie, R. C. *Journal of General Physiology* **117**(1), 3–25 (2001). Cited By (since 1996): 27.
18. Ljung, L. *System Identification - Theory for the User*. Prentice Hall, Linköping University, Sweden, 2 edition, (1999).
19. Juusola, M. and de Polavieja, G. G. *J. Gen. Physiol.* **122**(2), 191–206 July (2003).
20. Mocks, J., Gasser, T., and Tuan, P. *ELECTROENCEPHALOGR. CLIN. NEUROPHYSIOL.* **57**(6), 571–580 (1984).
21. Billings, S. and Leontaritis, I. *IEE Conference Publication, Warwick University* **194**, 183–187 (1981).
22. Leontaritis, I. J. and Billings, S. A. *International Journal of Control* **41**(2), 303–344 (1985).
23. Pearson, R. K. *Discrete-Time Dynamic Models*. Oxford University Press, (1999).
24. Wei, H., Billings, S., and Liu, J. *International Journal of Control* **77**(1), 86–110 (2004).
25. Chen, S., Billings, S. A., and Luo, W. *International Journal of Control* **50**(5), 1873–1896 (1989). Cited By (since 1996): 238.
26. Akaike, H. *Annals of the Institute of Statistical Mathematics* **21**(1), 243–247 December (1969).
27. Billings, S. A. and Zhu, Q. M. *International Journal of Control* **60**(6), 1107–1120 (1994).
28. Diaz, H. *Automatica* **24 (5)**, 629–641 (1988).
29. Volterra, V. *Theory of functionals and of integral and integro-differential equations*. Blackie, London, (1930).
30. Billings, S. A. and Tsang, K. M. *Mechanical Systems and Signal Processing* **3**(4), 341–359 October (1989).
31. Peyton-Jones, J. C. and Billings, S. A. *International Journal of Control* **50**(5), 1925–1940 (1989).
32. Gu, Y., Oberwinkler, J., Postma, M., and Hardie, R. C. *Current Biology* **15**(13), 1228–1234 July (2005).
33. Zheng, L., De Polavieja, G., Wolfram, V., Asyali, M., Hardie, R., and Juusola, M. *Journal of General Physiology* **127**(5), 495–510 (2006).
34. Chow, T., Hong-Zhou, T., and Yong, F. In *Encyclopedia of Electrical and Electronics Engineering*. Wiley (2001).
35. Zhao, X. and Marmarelis, V. *Math. Comput. Model.* **27**(5), 37–43 (1998).